Title: Mechanistic understanding of the summer precipitation and recent wetting trend over Northwest China and Mongolia

Authors: Yi Ming[1], Wenhao Dong[2,3], Yi Deng[4], Yongkun Xie[5], Zhaoyi Shen[6], Jianping Huang[7]

Affiliations:
[1]Schiller Institute for Integrated Science and Society and Department of Earth and Environmental Sciences, Boston College, Boston, MA
[2]Cooperative Programs for the Advancement of Earth System Science, University Corporation for Atmospheric Research, Boulder, CO
[3]NOAA/Geophysical Fluid Dynamics Laboratory, Princeton, NJ
[4]School of Earth and Atmospheric Sciences, Georgia Institute of Technology, Atlanta, GA
[5]State Key Laboratory of Numerical Modeling for Atmospheric Sciences and Geophysical Fluid Dynamics, Institute of Atmospheric Physics, Chinese Academy of Sciences, Beijing
[6]Department of Environmental Science and Engineering, California Institute of Technology, Pasadena, CA
[7]Key Laboratory for Semi-Arid Climate Change of the Ministry of Education, College of Atmospheric Sciences, Lanzhou University, Lanzhou

Key points:
- A hierarchical clustering analysis reveals three distinct summer precipitation patterns over Northwest China and Mongolia.
- Strong precipitation events are triggered by the upper-tropospheric disturbances in the form of transient Rossby wave packets.
- The recent wetting trend is attributed to more frequent strong precipitation events over the eastern part of the region.

Corresponding author: Yi Ming, mingy@bc.edu

Abstract

The arid region of Northwest China and Mongolia (NCM) receives most of the precipitation in the summer. The need for a better understanding of the synoptic-scale mechanism responsible for precipitation formation is accentuated by the recent wetting trend and its implications for future hydroclimate change. By conducting a hierarchical clustering analysis on an observationally-based daily precipitation dataset, we show that there are three distinct precipitation patterns over NCM, one of which is associated with strong precipitation over the western part of the region and another over the eastern part. The corresponding large-scale circulation anomalies indicate that these strong precipitation events are triggered by the upper-tropospheric disturbances in the form of transient Rossby wave packets. Furthermore, the wetting trend is linked to more frequent strong precipitation events over the eastern NCM, suggesting that it may have been induced remotely by atmospheric circulation perturbations.

Plain Language Summary

One of the world's driest regions, Northwest China and Mongolia has seen a significant increase in summer precipitation in the last few decades. The wetting trend has generally been thought of as a superposition of large-scale circulation changes and long-term atmospheric moistening as Earth's climate warms. However, the underlying cause is yet to emerge due to insufficient understanding of the summer precipitation formation on the weather scale. In this study, we apply a hierarchical clustering algorithm to the observed daily precipitation to identify the main spatial patterns. A key finding is that there are three distinct daily precipitation patterns, two of which are associated with strong precipitation events. By analyzing the intensity, duration, and frequency of these events, we also show that the wetting trend results primarily from more frequent events over the eastern part of the region. A detailed analysis of the associated large-scale circulation patterns demonstrates that strong precipitation events over NCM are initiated by the upper-tropospheric disturbances originating from other regions thousands of kilometers away. The results point to new directions in which one can better understand the root cause of the observed wetting trend, and project future changes.

1. Introduction

Far from the ocean and surrounded by mountain ranges, Northwest China and Mongolia (NCM, defined approximately as 80°–110°E and 35°–50°N) is home to the vast Taklamakan and Gobi Deserts (Fig. 1a). Although with an annual-mean precipitation of only 0.45 mm d^{-1} the region is considered arid, the distribution of precipitation is highly uneven both temporally and spatially. Most precipitation falls in the summer (June, July and August or JJA) (Baldwin & Vecchi, 2016), which is the focus of this work. Orography plays a central role in determining the spatial distribution of the summer precipitation (Fig. 1b). The mountainous areas receive about 1–2 mm d^{-1} during the season, which is key to sustaining local glaciers and grasslands.

A multi-decadal (1961–2010) wetting trend over Northwest China has been discussed based primarily on sparse station data in the literature (Peng & Zhou, 2018, and references therein), but is not borne out in the widely used global precipitation datasets (Fig. S1 in the Supporting Information). Instead, this study focuses on the latest two decades (2000–2019), for which the observations are more abundant and reliable, and there is indeed a robust wetting trend. It manifests mainly over the eastern part of NCM (to the east of the Khangai Mountains and the Qilian Mountains) (Fig. 1c). The regional-mean summer precipitation has a linear trend of 0.36 mm d^{-1} (20 yr)$^{-1}$, which amounts to 35% of the climatological precipitation (Fig. 1d). Note that the trend analysis presented here is based on the NOAA/Climate Prediction Center (CPC) dataset (see Fig. S2 for other global datasets and station data).

A clear picture of the underlying cause of the wetting trend is yet to emerge. Possible contributing factors include the local enhancement of convective instability (Zhou & Huang, 2010), and the remote influences of weaker South Asian summer monsoon (Y. Zhao et al., 2014) and stronger subtropical high pressure systems (Li et al., 2016). Attempts were also made to link the wetting to global warming (e.g. Shi et al., 2007), but without strong evidences. The inability to attribute the observed multi-decadal wetting trend over NCM is rooted fundamentally in the lack of understanding of the summer precipitation formation on the synoptic scale. If viewing the issue from the relative importance of dynamic versus thermodynamic processes, one would naturally expect the former to play a more prominent role over an arid (moisture-poor) region than over a wet (moisture-rich) region (such as monsoonal regions). In this sense, it would be difficult to generate insights from analyses on local atmospheric instability (Zhou & Huang, 2010) and moisture sources (Peng & Zhou, 2018). G. Chen and Huang (2012) examined the connections between the interannual variations of the summer precipitation over Northwest China and large-scale atmospheric circulation patterns, and identified two major teleconnection pathways realized through stationary Rossby waves, namely the circumglobal (zonal) or Silk Road and the Europe-China (meridional) modes. Although these results may not be directly applicable to the synoptic scale, they highlight the need to better elucidate the role of large-scale dynamics in studying the hydroclimate of arid and semi-arid regions. Rossby wave breaking and associated intense moisture transport, atmospheric rivers being an important manifestation, are known to cause extreme precipitation events over arid regions such as the Middle East and Southwest United States, but NCM is not a hot spot for wave breaking (De Vries, 2021). The goal of this work is to illustrate the physical mechanism of the summer precipitation formation over NCM, and to understand the nature of the past wetting trend (natural versus forced) and possible implications for projecting future changes.

2. Methods

This study uses the NOAA/CPC Global Daily Unified Gauge-Based Analysis of Precipitation, which covers 1979–2019 at a horizontal resolution of 0.5°×0.5° (M. Chen et al., 2008). Multi-level daily horizontal winds, geopotential height, specific humidity and temperature from the ERA-Interim reanalysis (Dee et al., 2011), at a horizontal resolution of 2°×2°, are also used to compute the large-scale circulation anomalies and covariance terms such as moisture flux and wave flux activity, the latter of which is used to quantify the role of atmospheric waves in energy and momentum transport, providing insights into the mechanisms that drive weather and climate patterns (Takaya and Nakamura, 2001).

A hierarchical clustering algorithm is applied to all summer precipitating days to identify prevailing spatial patterns. Precipitating days are defined to be those in the 99th percent of all the domain-average daily precipitation distribution; the cutoff value is approximately 0.1 mm d^{-1}. To maximize the sample size, the entire length of the CPC dataset (41 years) is used. This translates to a total of 3734 summer precipitating days (41×92×0.99). Each precipitating day is initially considered as a single-element cluster. The pair of clusters with the greatest similarity are then merged. Note that similarity is measured with Ward's minimum variance method (Ward, 1963), which minimizes the total within-cluster variance. This procedure is repeated until every precipitating day becomes a member of a large cluster. The optimal number of clusters is determined by maximizing the average silhouette approach. The large-scale circulation patterns associated with each cluster are constructed by compositing the daily anomalies with respect to the mean values of the 99th-percentile days rather than those of all days (the JJA climatology). This type of clustering analysis has been performed widely for classifying precipitation patterns. For example, S. Zhao et al. (2016, 2017) used it to identify the spatial structures of extreme precipitation events over the contiguous United States.

A precipitation event here refers to one or more consecutive precipitation days that fall into one of the identified clusters occurs. Its duration is simply the number of the consecutive days, and its intensity is the average precipitation over these days. For each summer, the frequency of precipitation events in a certain cluster is the total number of precipitation events, while the duration and intensity are averaged over these events.

3. Results

The clustering procedure yields an optimal number of three clusters for the summer precipitation over NCM, referred to as C1, C2 and C3. C1 accounts for most of the precipitating days (71%), while C2 and C3 are roughly of equal weights (14% and 15%, respectively). Their probability density distributions are given in Fig. S3. The top row of Fig. 2 shows that the precipitation rates on C1 days, with a domain-average of 0.8 mm d^{-1}, are biased low almost everywhere in the study region, and there are no coherent large-scale circulation anomalies. By contrast, both C2 and C3 days feature intense precipitation (averaged at 2.1 and 1.8 mm d^{-1}, respectively), but at different locations. The C2-associated precipitation is primarily over the western part of NCM, while C3 favors the eastern part. In both cases, there is a pronounced cyclonic circulation at 500 hPa over NCM, accompanied by an anticyclonic circulation to the northwest and another to the east.

The anomalies in precipitation are in good agreement with those in 700-hPa moisture flux convergence in terms of spatial distribution (the middle row of Fig. 2), suggesting that local evaporation plays a minor role. For C2, moisture seems to originate mainly from the South Asian monsoon region. For C3, the East Asian monsoon region appears to be the main source as moisture transport vector over South Asia is quite small. The alternating positive and negative anomalies in 500-hPa geopotential height in C2 and C3 seen in the third row of Fig. 2 are reminiscent of Rossby wave trains (zonal wavenumber ~5). As indicated by the wave activity flux, the zonal propagation is from west to east across Eurasia in both cases. On the other hand, the poleward propagation is more pronounced in C2 than in C3. Interestingly, C2 is of larger amplitude than C3. Lutsko and Held (2006) showed that the stationary Rossby waves excited by idealized mountains changes from being circumglobal (zonal) to being more meridional as the amplitude increases. The reason is that stronger waves can alter the mid-latitude jet, which serves as waveguide in the circumglobal case. The results presented here seem to be consistent, but more detailed analysis is needed to ascertain that the same mechanisms hold.

The vertical structures of the geopotential height anomalies are barotropic in the upper troposphere (above ~500 hPa) (Fig. 3), as one would expect for Rossby waves. The time evolution shows that they are transient in nature. From Day -2 to Day 0, the upper-tropospheric trough moves from upstream into NCM, intensifying along the way. It continues to propagate eastward, and weakens significantly by Day 2. Another interesting observation is that the lower-tropospheric anomalies are baroclinic and tilted against the vertical wind shear around the study region. This suggests that the upper-tropospheric Rossby wave packets can excite baroclinic waves in the lower troposphere. The slantwise convection associated with the latter is the mechanistic driver of intense precipitation over NCM.

One can decompose the summer precipitation into the contributions from different cluster. Although C1 accounts for most of the climatological precipitation, the 2000–2019 wetting trend is attributed mainly to C3, and to a lesser extent, to C2 (Fig. 4a). The former is statistically significant, while the latter is not. This is consistent with the fact that the wetting trend is more pronounced over the eastern part of NCM (Fig. 1c). The contribution from C1 is effectively unchanged during the two decades. The time series of the main characteristics of each cluster, namely frequency, duration and intensity, are shown in Figs. 4b-d. The increase in C3-associated precipitation is mainly due to more frequent occurrence. The linear trend of 7.73 (20 yr)$^{-1}$ amounts to about 70% of the climatological value. C1 days are also more frequent, but the corresponding duration decreases substantially. These two factors cancel out and results in no net change in precipitation. The duration does not change for C2 and C3. Although the increasing intensity of C1 and C2 is not enough to alter their respective precipitation trends (Fig. 4a), it would be worthwhile to further investigate the controlling factors of the precipitation intensity. A good starting point may be to separate the thermodynamic and dynamic effects.

4. Discussion

An insight from this work is that the upper-tropospheric disturbances in the form of transient Rossby waves packets are key to inducing strong precipitation over NCM. The two wave types (C2 and C3), which differ in the relative importance of the meridional versus zonal propagation, are reminiscent of the Europe-Asia and circumglobal teleconnections discussed in G. Chen and Huang (2012), even though the latter operate at the interannual time scale and are realized through stationary Rossby waves. This indicates that similar mechanisms may be involved at the synoptic scale. A prominent feature of the Northern Hemisphere summer circulation is the Asian jet stream. A large body of literature (Lutsko & Held, 2016, and references therein) exists on how a jet can act as waveguide to induce circumglobal Rossby waves under certain conditions. This deviates from the canonical picture that Rossby waves propagate both poleward and equatorward along great circles until they are absorbed and/or reflected near the critical lines (Hoskins & Karoly, 1981). This work shows that both mechanisms contribute approximately equally to the long-term average summer precipitation over NCM, but the circumglobal mode (C3) plays an outsize role in causing the wetting trend in the last two decades. It is not entirely clear how the two wave types interact with each other, and what factors determine their relative importance over NCM.

It is well known that multiple sources can give rise to multi-decadal atmospheric variability. One possibility is the nonlinearity of internal atmospheric dynamics in the absence of boundary forcings (James & James, 1989). High-frequency atmospheric noise has been shown to play a crucial role in driving low-frequency variability in the coupled atmosphere-ocean system, a leading example involving the North Atlantic Oscillation (NAO) and Atlantic Multidecadal Variability (AMV) (Clement et al., 2015; Delworth et al., 2017). External forcings such as greenhouse gases and the solar cycle can also be involved. Note that the latter two effects are usually associated with low-frequency variations in sea-surface temperatures (SST), which play a crucial role in determining diabatic heating. Attribution of the observed wetting trend over NCM is a challenging task without conducting climate model simulations, which will be analyzed in a subsequent study.

Although the recent wetting trend may not persist or even reverse, one cannot discount possible influence of anthropogenic climate change on the long-term hydroclimate of NCM. Chemke and Ming (2020) showed that the overall response of mid-latitude eddy kinetic energy (EKE) to global warming varies with zonal wavenumber; large waves become stronger, while small waves weaker. All wavenumbers, however, undergo substantial decreases in JJA (see their Fig. S5). One would naturally expect a drying of NCM. On the other hand, weaker waves may favor the circumglobal mode more, a change that may bring more precipitation to the eastern part of NCM. It would be interesting to further investigate these factors. One should also pay special attention to any change in the summer Asian jet, which is important for understanding Rossby wave propagation. Note that the current climate model ensemble projects very little changes in the location and strength of the jet (Chowdary et al., 2019). On the thermodynamic side, the increase in atmospheric moisture content with temperature (i.e. the Clausius-Clapeyron scaling) has to be taken into account.

Acknowledgements

We thank Drs. Ming Zhao and Akshaya Nikumb for commenting on an earlier version of the paper. Wenhao Dong's contribution at Geophysical Fluid Dynamics Laboratory is supported by NOAA's Science Collaboration Program and administered by UCAR's Cooperative Programs for the Advancement of Earth System Science (CPAESS) under awards NA16NWS4620043 and NA18NWS4620043B.

Open Research

The NOAA CPC Global Unified Gauge-Based Analysis of Daily Precipitation dataset can be found at https://psl.noaa.gov/data/gridded/data.cpc.globalprecip.html. For the ERA-Interim reanalysis datasets, they can be accessed from https://rda.ucar.edu/datasets/ds627.0/dataaccess/.

References

Baldwin, J., & Vecchi, G. (2016). Influence of the Tian Shan on arid extratropical Asia. *Journal of Climate*, 29 (16), 5741–5762.

Chemke, R., & Ming, Y. (2020). Large atmospheric waves will get stronger, while small waves will get weaker by the end of the 21st century. *Geophysical Research Letters*, 47 (22).

Chen, G., & Huang, R. (2012). Excitation mechanisms of the teleconnection patterns affecting the July precipitation in Northwest China. *Journal of Climate*, 25 (22), 7834–7851.

Chen, M., Shi, W., Xie, P., Silva, V. B. S., Kousky, V. E., Wayne Higgins, R., & Janowiak, J. E. (2008). Assessing objective techniques for gauge-based analyses of global daily precipitation. *Journal of Geophysical Research: Atmospheres*, 113 (D4).

Chowdary, J. S., Hu, K., Srinivas, G., Kosaka, Y., Wang, L., & Rao, K. K. (2019). The Eurasian jet streams as conduits for east Asian monsoon variability. *Current Climate Change Reports*, 5 (3), 233–244.

Clement, A., Bellomo, K., Murphy, L. N., Cane, M. A., Mauritsen, T., Rädel, G., & Stevens, B. (2015). The Atlantic Multidecadal Oscillation without a role for ocean circulation. *Science*, 350 (6258), 320–324.

Dee, D. P., Uppala, S. M., Simmons, A. J., Berrisford, P., Poli, P., Kobayashi, S., . . .Vitart, F. (2011). The ERA-Interim reanalysis: configuration and performance of the data assimilation system. *Quarterly Journal of the Royal Meteorological Society*, 137 (656), 553–597.

Delworth, T. L., Zeng, F., Zhang, L., Zhang, R., Vecchi, G. A., & Yang, X. (2017). The central role of ocean dynamics in connecting the North Atlantic Oscillation to the extratropical component of the Atlantic Multidecadal Oscillation. *Journal of Climate*, 30(10), 3789–3805.

De Vries, A. J. (2021). A global climatological perspective on the importance of Rossby wave breaking and intense moisture transport for extreme precipitation events. *Weather and Climate Dynamics*, 2 (1), 129–161.

Hoskins, B. J., & Karoly, D. J. (1981). The steady linear response of a spherical atmosphere to thermal and orographic forcing. *Journal of the Atmospheric Sciences*, 38 (6), 1179–1196.

James, I., & James, P. (1989). Ultra-low-frequency variability in a simple atmospheric circulation model. *Nature*, 342 (6245), 53–55.

Li, B., Chen, Y., Chen, Z., Xiong, H., & Lian, L. (2016). Why does precipitation in northwest China show a significant increasing trend from 1960 to 2010? *Atmospheric Research*, 167, 275–284.

Lutsko, N. J., & Held, I. M. (2016). The response of an idealized atmosphere to orographic forcing: Zonal versus meridional propagation. *Journal of the Atmospheric Sciences*, 73 (9), 3701–3718.

Peng, D., & Zhou, T. (2018). Why was the arid and semiarid northwest China getting wetter in the recent decades? *Journal of Geophysical Research: Atmospheres*, 122 (17), 9060–9075.

Shi, Y., Shen, Y., Kang, E., Li, D., Ding, Y., Zhang, G., & Hu, R. (2007). Recent and future climate change in northwest China. *Climatic Change*, 80 (3), 379–393.

Takaya, K., & Nakamura, H. (2001). A formulation of a phase-independent wave-activity flux for stationary and migratory quasi geostrophic eddies on a zonally varying basic flow. *Journal of the Atmospheric Science*, 58 (81), 608–627.

Ward, J. H. (1963). Hierarchical Grouping to Optimize an Objective Function. *Journal of the American Statistical Association*,58(301), 236–244.

Zhao, S., Deng, Y., & Black, R. X. (2016). Warm season dry spells in the central and eastern United States: Diverging skill in climate model representation. *Journal of Climate*, 29 (15), 5617–5624.

Zhao, S., Deng, Y., & Black, R. X. (2017). A dynamical and statistical characterization of US extreme precipitation events and their associated large-scale meteorological patterns. *Journal of Climate*, 30 (4), 1307–1326.

Zhao, Y., Huang, A., Zhou, Y., Huang, D., Yang, Q., Ma, Y., . . . Wei, G. (2014). Impact of the middle and upper tropospheric cooling over central Asia on the summer rainfall in the Tarim Basin, China. *Journal of Climate*, 27 (12),2704721–4732.

Zhou, L. T., & Huang, R. H. (2010). Interdecadal variability of summer rainfall in Northwest China and its possible causes. *International Journal of Climatology*, 30 (4), 549–557.

Figures

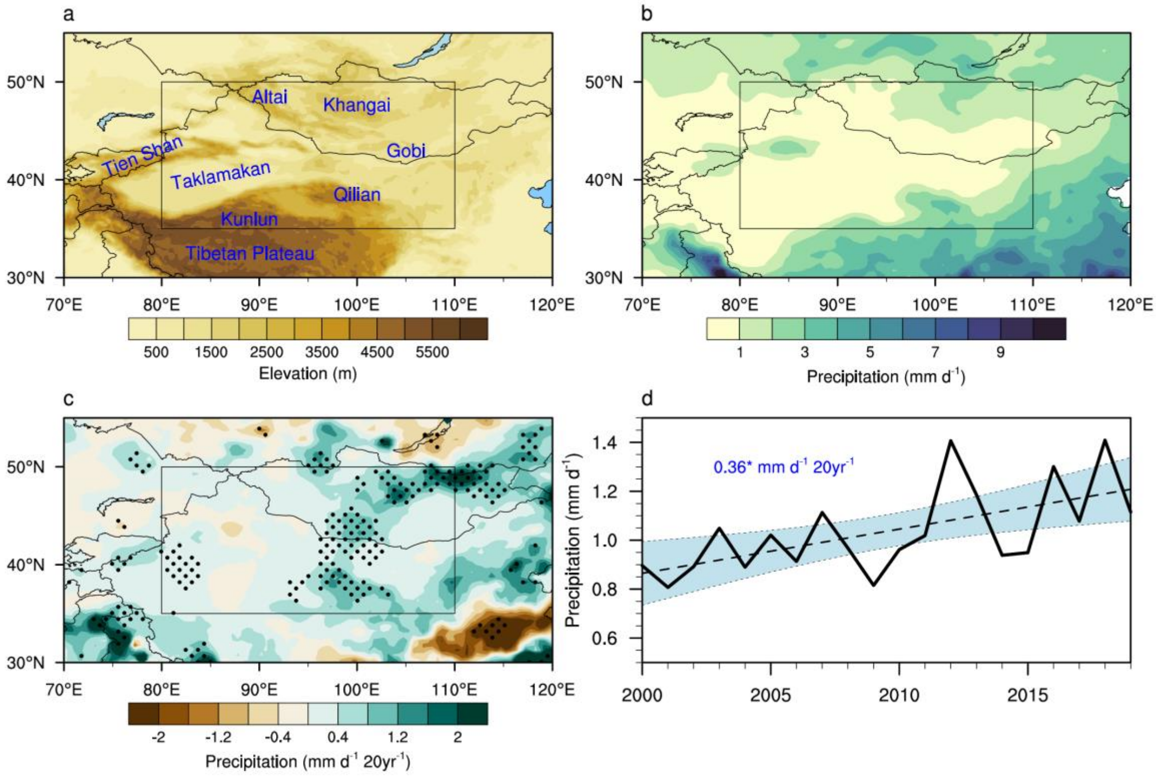

Figure 1. (a) Elevation of the study region, with the main geologic features (i.e. deserts and mountain ranges) labeled in blue, and Northwest China and Mongolia (NCM) defined approximately as 80°–110°E and 35°–50°N (the black rectangle). (b) Spatial distribution of the summer mean precipitation (2000-2019). (c) Spatial distribution of the linear trend of the summer precipitation (2000-2019). Stippling denotes statistical significance at the 95% confidence level. (d) Time series of the NCM-average summer precipitation. The best linear fit and prediction errors are represented by the black dashed line and blue shading, respectively. The linear trend is given, with an asterisk denoting statistical significance at the 95% confidence level.

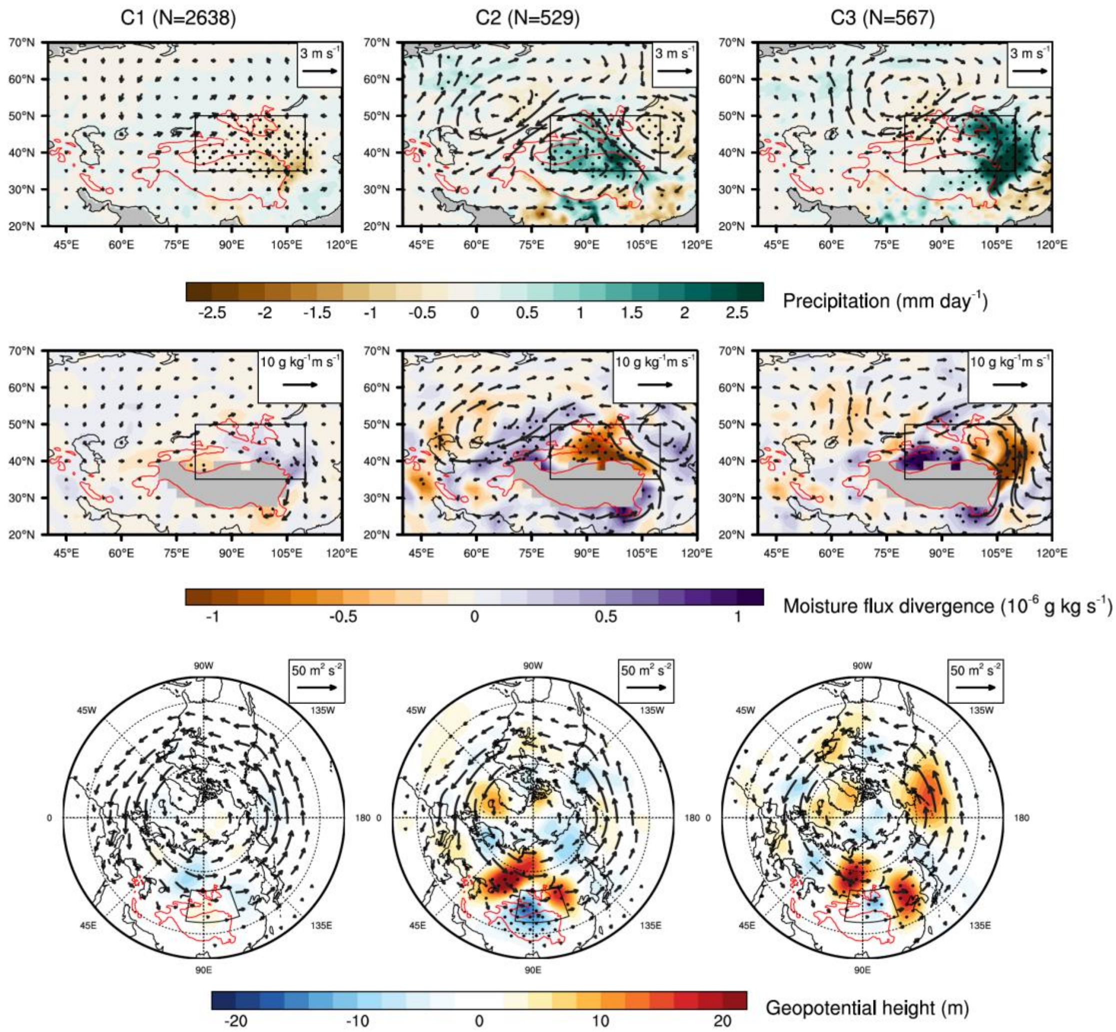

Figure 2. Composite anomalies for the three clusters (one column for each cluster). *N* is the number of samples in each cluster. Top row: precipitation (shadings) overlaid with 500-hPa winds (arrows). Middle row: 700-hPa moisture flux divergence (shadings) overlaid with moisture flux (arrows). Bottom row: 500-hPa geopotential height (shadings) overlaid with wave activity flux (arrows). Black rectangle denotes NCM while gray shading in the first two rows denotes regions where the data are not available.

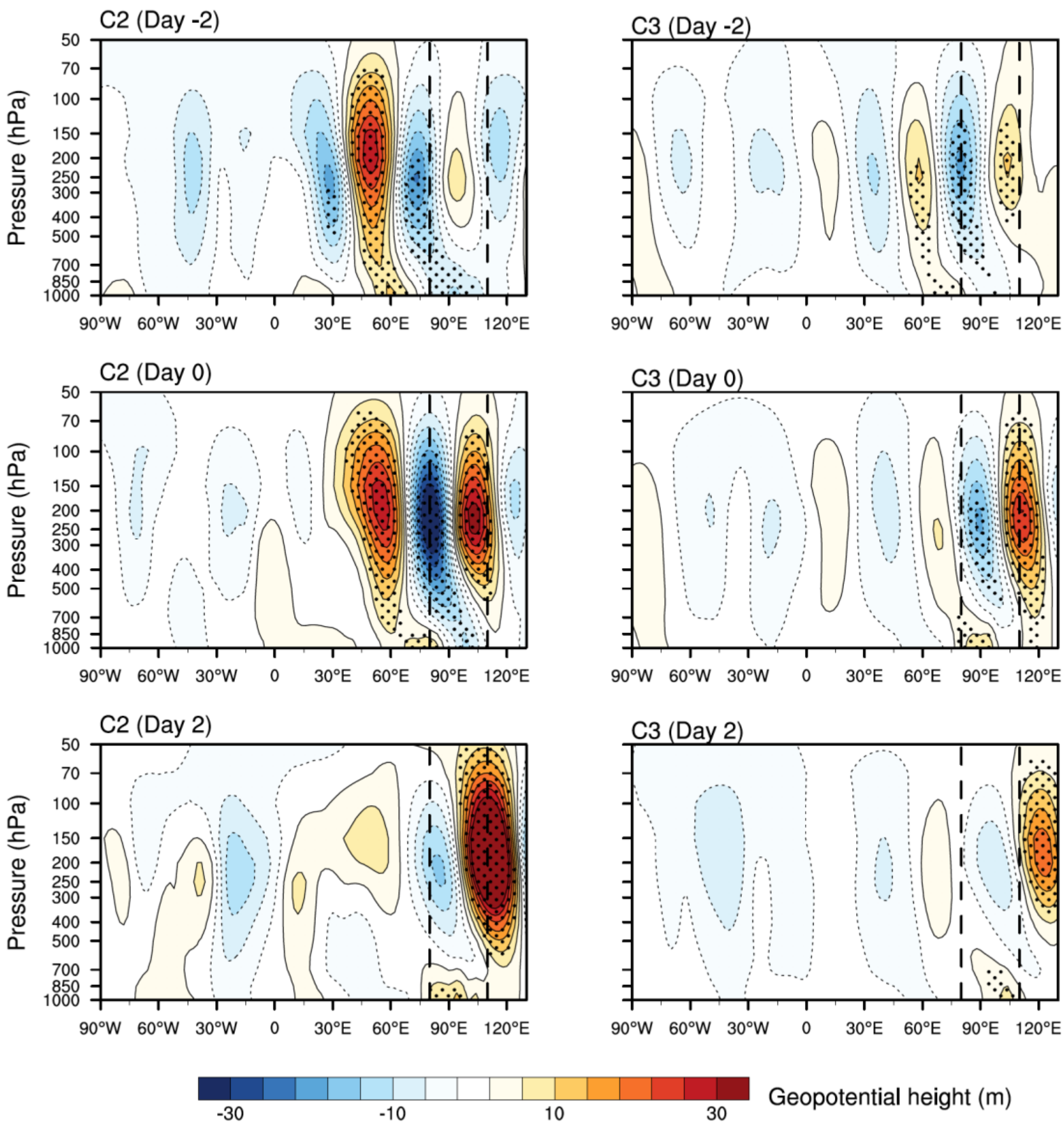

Figure 3. Vertical structures of the composite anomalies in geopotential height averaged over 30°–50°N on Day -2 (top row), 0 (middle row) and 2 (bottom row) in C2 (left column) and C3 (right column). Vertical dash lines are the longitudinal boundaries for NCM.

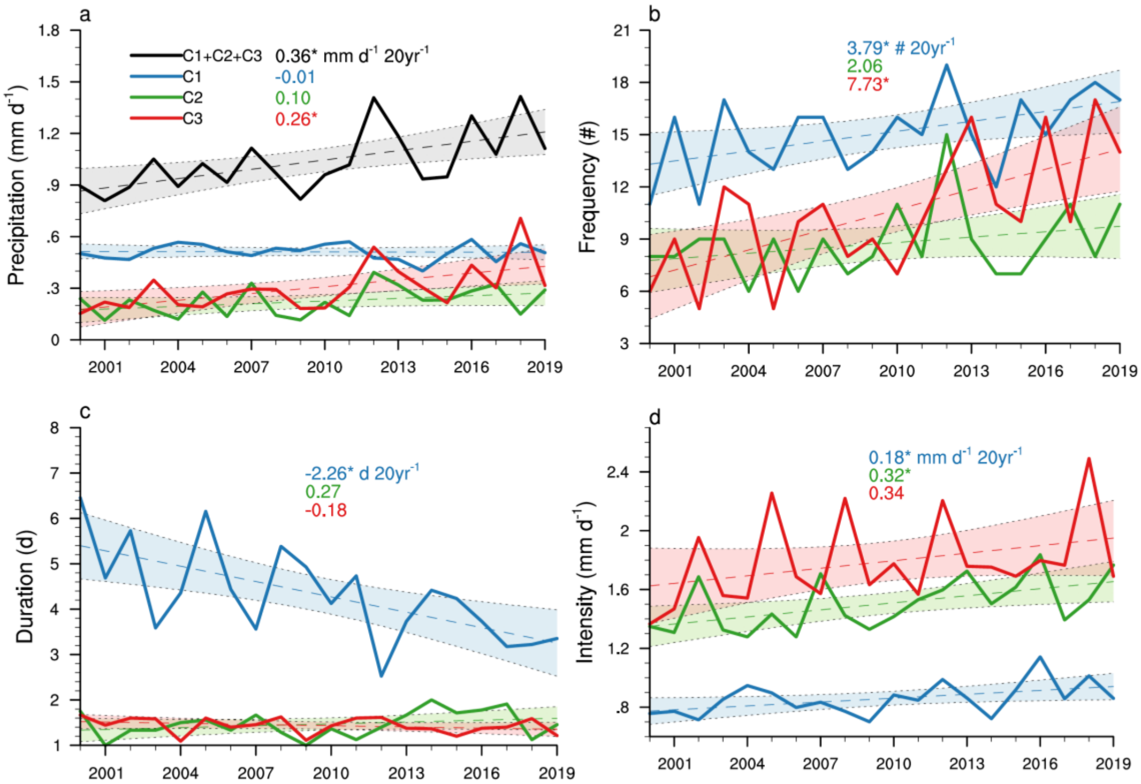

Figure 4. Time series of the (a) combined precipitation, (b) frequency, (c) duration and (d) intensity of the three clusters. For each series, the best linear fit and prediction errors are represented by the dashed line and shading, respectively. The linear trends are given, with asterisks denoting statistical significance at the 95% confidence level.